The Journal of Chemical Physics

RESEARCH ARTICLE | MAY 28 2024

The eXact integral simplified time-dependent density functional theory (XsTD-DFT)

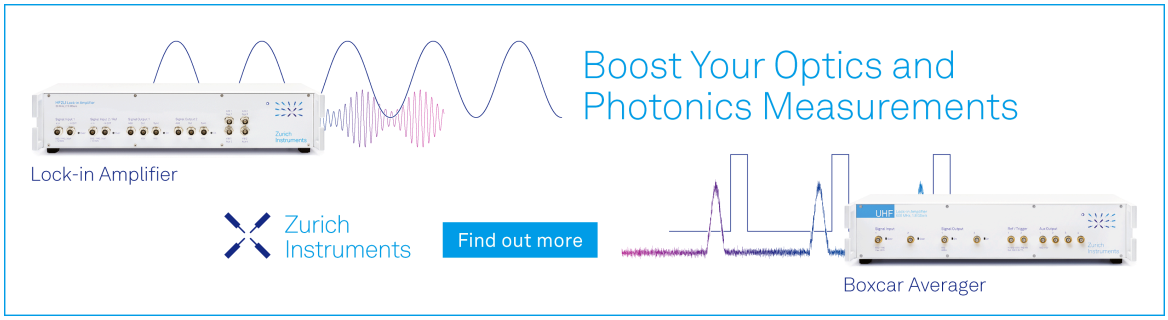
Marc de Wergifosse ; Stefan Grimme

Check for updates

J. Chem. Phys. 160, 204110 (2024)
https://doi.org/10.1063/5.0206380

View Online
Export Citation

29 May 2024 06:59:37



AIP Publishing

The Journal of Chemical Physics ARTICLE pubs.aip.org/aip/jcp

The eXact integral simplified time-dependent density functional theory (XsTD-DFT)

Cite as: J. Chem. Phys. 160, 204110 (2024); doi: 10.1063/5.0206380
Submitted: 1 March 2024 • Accepted: 5 May 2024 •
Published Online: 28 May 2024

View Online Export Citation CrossMark

Marc de Wergifosse[1,2,a)] and Stefan Grimme[2]

AFFILIATIONS

[1] Theoretical Chemistry Group, Molecular Chemistry, Materials and Catalysis Division (MOST), Institute of Condensed Matter and Nanosciences, Université Catholique de Louvain, Place Louis Pasteur 1, B-1348 Louvain-la-Neuve, Belgium
[2] Mulliken Center for Theoretical Chemistry, Institut für Physikalische und Theoretische Chemie, Beringstr. 4, 53115 Bonn, Germany

Note: This paper is part of the 2024 JCP Emerging Investigators Special Collection.
[a)] **Author to whom correspondence should be addressed:** marc.dewergifosse@uclouvain.be

ABSTRACT

In the framework of simplified quantum chemistry methods, we introduce the eXact integral simplified time-dependent density functional theory (XsTD-DFT). This method is based on the simplified time-dependent density functional theory (sTD-DFT), where all semi-empirical two-electron integrals are replaced by exact one- and two-center two-electron integrals, while other approximations from sTD-DFT are kept. The performance of this new parameter-free XsTD-DFT method was benchmarked on excited state and (non)linear response properties, including ultra-violet/visible absorption, first hyperpolarizability, and two-photon absorption (2PA). For a set of 77 molecules, the results from the XsTDA approach were compared to the TDA data. XsTDA/B3LYP excitation energies only deviate on average by 0.14 eV from TDA while drastically cutting computational costs by a factor of 20 or more depending on the energy threshold chosen. The absolute deviations of excitation energies with respect to the full scheme are decreasing with increasing system size, showing the suitability of XsTDA/XsTD-DFT to treat large systems. Comparing XsTDA and its predecessor sTDA, the new scheme generally improves excitation energies and oscillator strengths, in particular, for charge transfer states. TD-DFT first hyperpolarizability frequency dispersions for a set of push-pull π-conjugated molecules are faithfully reproduced by XsTD-DFT, while the previous sTD-DFT method provides redshifted resonance energy positions. Excellent performance with respect to the experiment is observed for the 2PA spectrum of the enhanced green fluorescent protein. The obtained robust accuracy similar to TD-DFT at a fraction of the computational cost opens the way for a plethora of applications for large systems and in high throughput screening studies.

Published under an exclusive license by AIP Publishing. https://doi.org/10.1063/5.0206380

29 May 2024 06:59:37

I. INTRODUCTION

The computation of molecular properties involving the interaction of light with matter using quantum chemistry (QC) methods remains challenging for large systems that are of timely interest. An ideal method should enable the treatment of open shell systems that may present multi-configurational character[1,2] and be able to compute excitations in vertical and adiabatic regimes. Considering linear and nonlinear optical response properties, the computation of such higher-order quantities is computationally involved and often needs a proper treatment of electron correlation effects, frequency dispersion, and explicit account of the environment.[3,4] Such methods exist but only for small systems.

If used with care, the time-dependent density functional theory (TD-DFT)[5–8] provides a reasonable route for the computation of excited states and response properties for medium-sized systems. However, it introduces substantial errors for several types of excitations involving charge-transfer (CT), double excitation, or Rydberg characters when using standard exchange–correlation (XC) functionals.[9] Even so, in many applications, it works well for low-lying valence states.[9] Considering large systems with a high density of excited states, it is not really necessary to describe individual excitations with high accuracy, and a TD-DFT treatment, including only singly excited configurations, might be sufficient.

A decade ago, the simplified time-dependent density functional theory (sTD-DFT) and its variant using the Tamm–Dancoff

Published under an exclusive license by AIP Publishing

approximation (sTDA) were introduced by one of us.[10,11] These approaches were extended to range-separated hybrid (RSH) functionals by Risthaus *et al.*[12] These methods were originally designed to evaluate the ultra-violet/visible (UV/vis) and circular dichroism (CD) spectra of large molecules (<1000 atoms) for which it was not possible to use conventional TD-DFT. In 2016, these methods were extended to ultra-large systems with the extended tight-binding (xTB) variant,[13] enabling the computation of excited states for organic systems with up to 5000 atoms and, more recently, to compounds with 4d and 5d metals as well as heavy p-block elements.[14] Since then, the reach of these simplified QC (sQC) methods was expanded to response properties allowing the evaluation of the polarizability,[15] optical rotation,[16] excited state absorption (ESA),[17] first hyperpolarizability,[15] and two-photon absorption (2PA).[18]

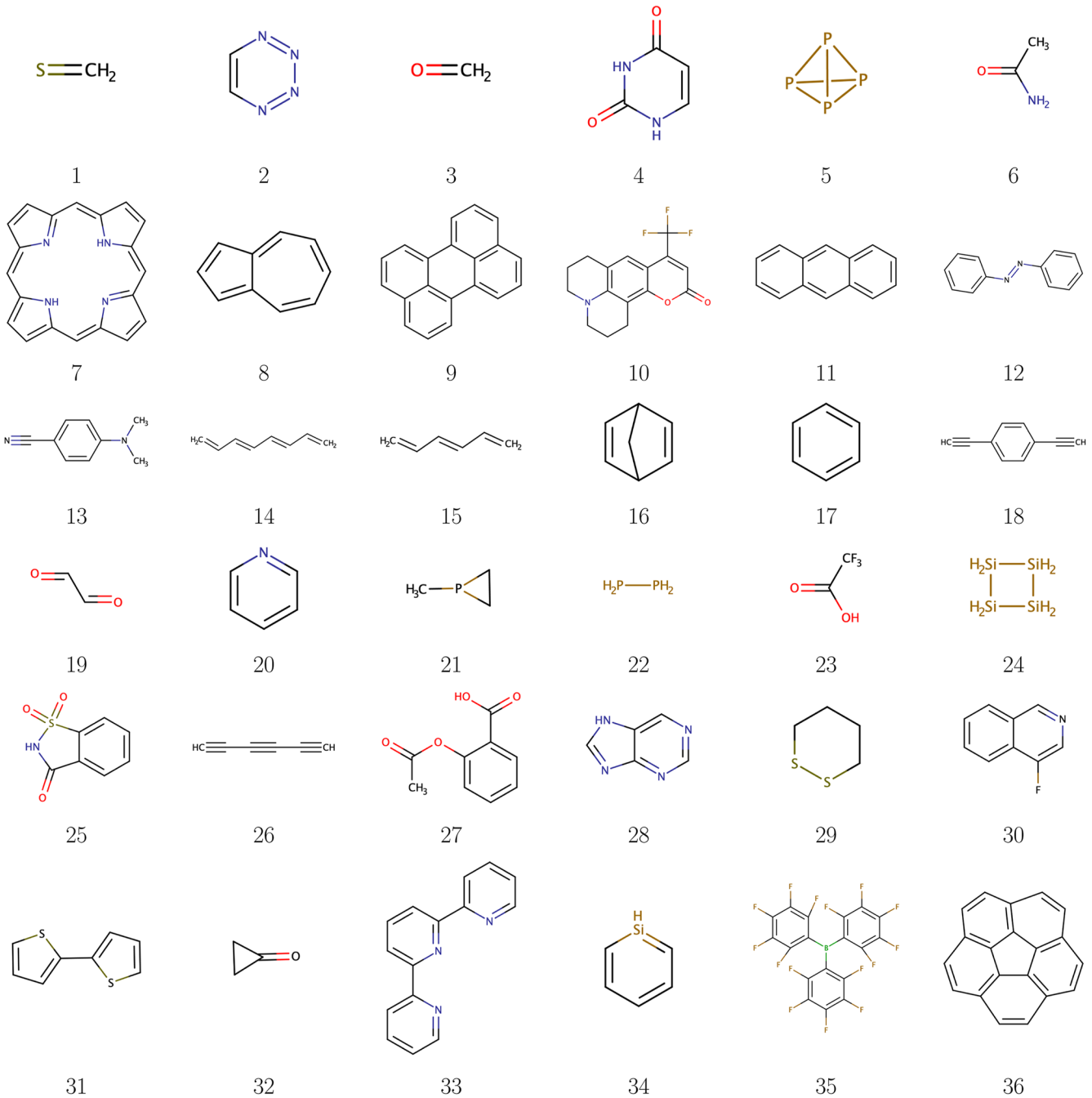


FIG. 1. Chemical structures of molecules 1 to 36 from the benchmark set of 77 molecules (**1–17**,[11] **18–20**,[12] **21–46**,[13] **47–57**,[34] and **58–77**[12]).

29 May 2024 06:59:37

Published under an exclusive license by AIP Publishing

A spin-flip variant[19] was also implemented and analysis tools involving natural transition/response orbitals to interpret excited states[20] and response properties.[21]

Here, sTD-DFT/sTDA methods also inspired alternative schemes to speed-up the excited state calculations. In 2016, Rüger *et al.*[22] proposed the TD-DFT+TB method. The TD-DFT+TB scheme, which is also based on a DFT ground state, uses a similar monopole approximation in the linear response treatment but considers local XC functionals instead of hybrid ones. Asadi-Aghbolaghi *et al.*[23] showed that the TD-DFT+TB method is up to 100 times faster than TD-DFT to evaluate excited states of large gold and silver plasmonic nanoparticles with less than 0.15 eV of error with respect to TD-DFT for excitation energies. Recently, Havenridge *et al.*[24] extended this method to the efficient computation of the analytical excited state gradient using the Z-vector method. Giannone and Della Sala[25] proposed the TD-DFT-as method, TD-DFT using the resolution of identity (RI) with only one s-type Gaussian basis function per atom. They argued that

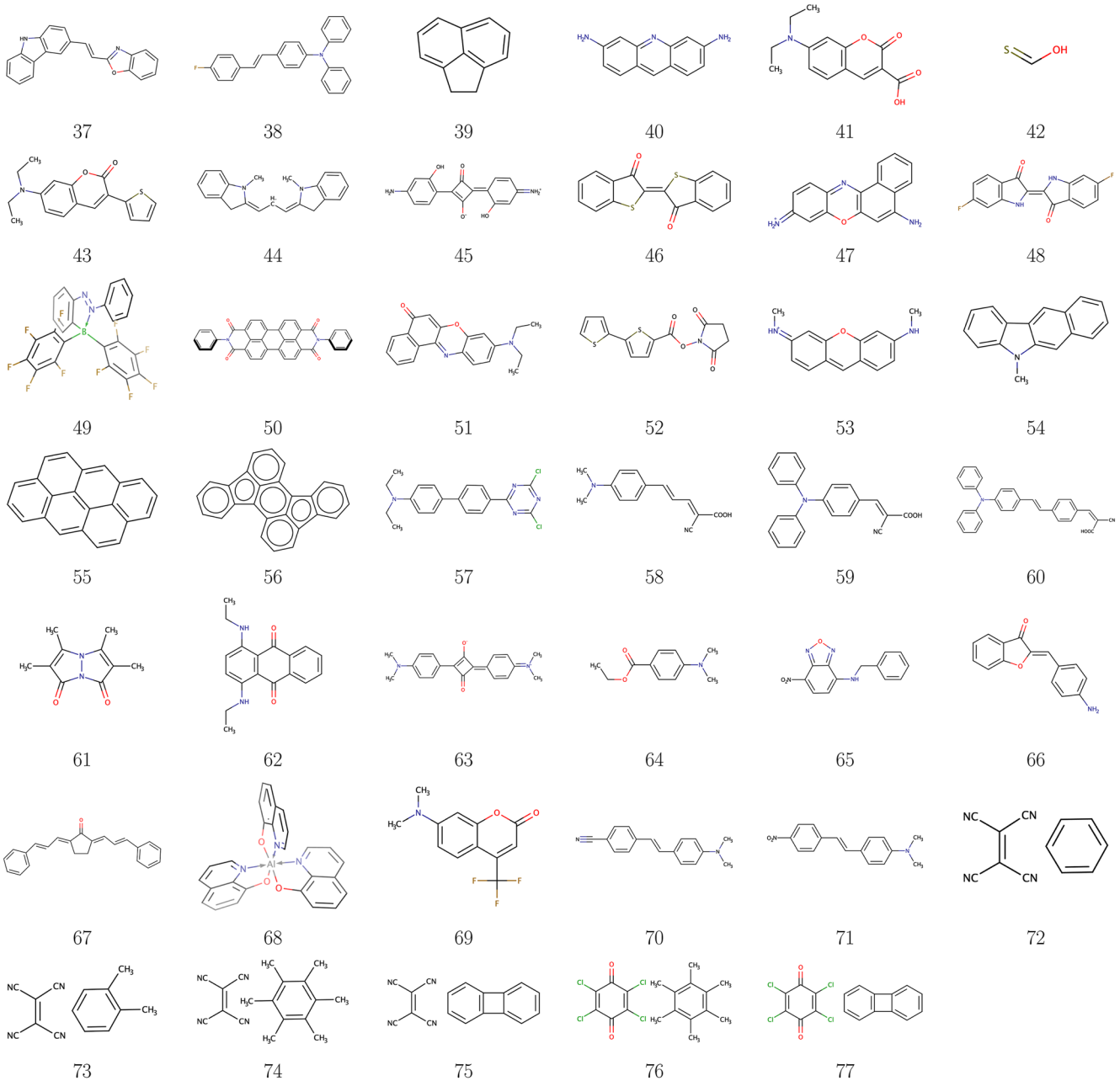


FIG. 2. Chemical structures of molecules **37–77** from the benchmark set of 77 molecules (**1–17**,[11] **18–20**,[12] **21–46**,[13] **47–57**,[34] and **58–77**[12]).

29 May 2024 06:59:37

Published under an exclusive license by AIP Publishing

sTD-DFT/sTDA/TD-DFT+TB can be seen as approximations to the TD-DFT-as method, where three-index RI two-electron integrals are replaced by Löwdin approximated ones. The TD-DFT-as approach was recently extended to hybrid XC functionals with the TD-DFT-ris method.[26] The use of a minimal auxiliary basis set with TD-DFT reduced the cost by around two orders of magnitude while reproducing the full scheme exceptionally well. Hehn *et al.*[27] added periodic boundary conditions to the sTDA scheme by splitting the Coulomb operator into a semiempirical short-range and an exact long-range contribution. A simplified GW/Bethe–Salpether equation (BSE) was also proposed by Cho *et al.*[28] in 2022.

In a perspective article,[29] we recently discussed future challenges for sQC methods. One idea was to improve the global accuracy of sQC schemes by going beyond its monopole approximation for the two-electron integrals. We explored this multipole approach but found an alternative route, which is the subject of this work. The sTD-DFT/sTDA approximated molecular orbital (MO) two-electron integrals use atomic transition charges obtained from a Löwdin orthogonalization procedure and the Mataga–Nishimoto–Ohno–Klopman (MNOK)[30–32] damped Coulomb operator, a function of the interatomic distance. To recover this, instead of using the MNOK operator, Löwdin-orthogonalized two-electron integrals $(\lambda_\alpha\lambda_\alpha|\lambda_\beta\lambda_\beta)$ are approximated by atomic orbital (AO) two-electron integrals $(\alpha\alpha|\beta\beta)$. By removing the semi-empirical nature of the two-electron integrals, we arrive to a more "*ab initio*" version of the sTD-DFT method where two-electron integrals in the zero differential overlap (ZDO) approximation[33] are computed exactly. This new method is introduced as the eXact integral simplified time-dependent density functional theory (XsTD-DFT), and its TDA variant (XsTDA) is also presented.

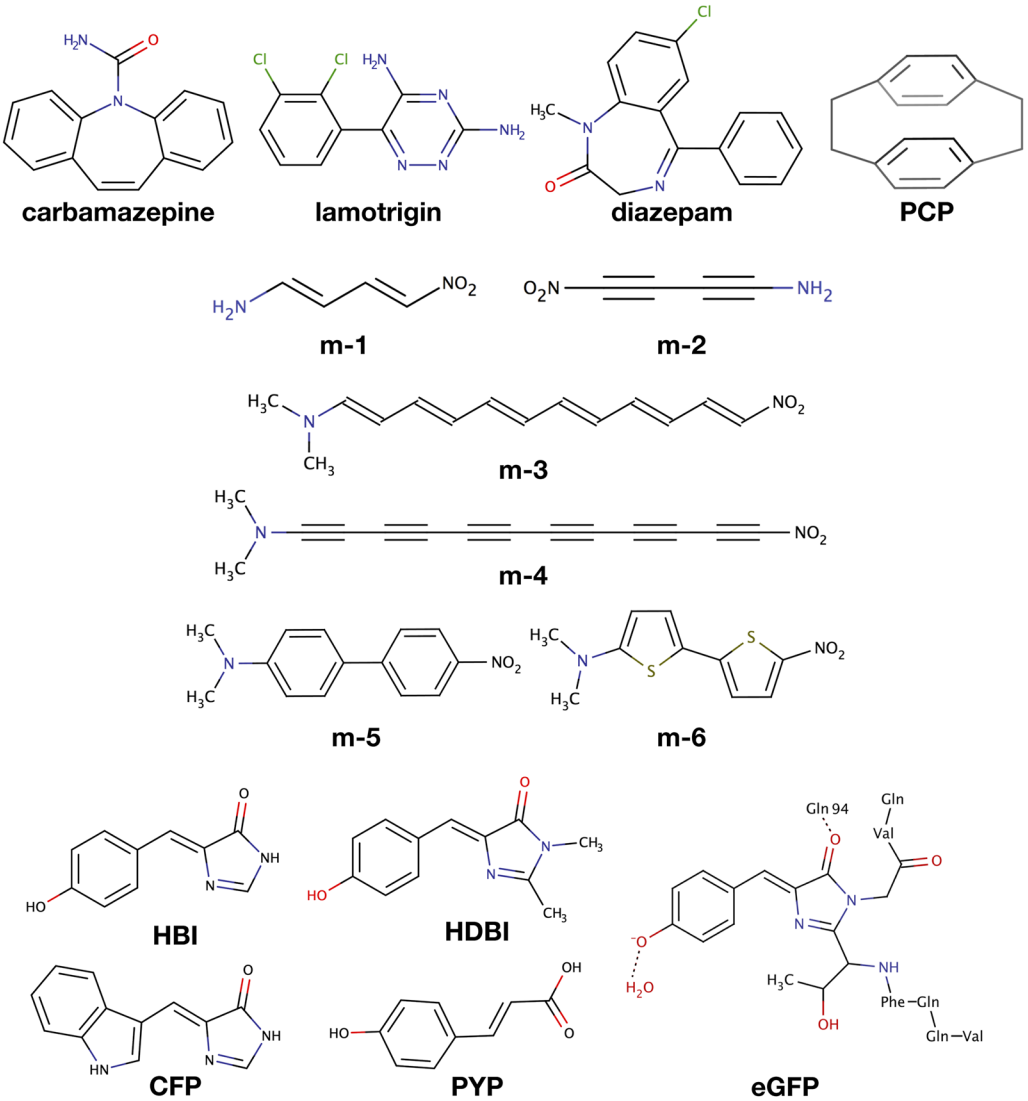


FIG. 3. Chemical structure of further considered systems: carbamazepine, lamotrigine, and diazepam *[2,2]-paracyclophane (PCP)*; six push-pull π-conjugated molecules; four FP chromphores (HBI, HBDI, CFP, and PYP); and the eGFP chromophore with its first shell of residues.

29 May 2024 06:59:37

Published under an exclusive license by AIP Publishing

To assess the performance of XsTDA for the evaluation of excited state energies and oscillator strengths, we benchmarked them with respect to the TDA results for a set of 77 molecules taken from earlier studies.[11–13,34] Figures 1 and 2 show the chemical structures of these systems. Note that this set includes the DYE12 test set,[34] which is composed of 12 large organic dyes and for which back-corrected "experimental" vertical excitation energies are available. This set also contains the mixed CT test set from Risthaus *et al.*[12] for which the reference SCS-CC2/def2-TZVP(-f) excitation energies are available. In addition, UV–vis absorption spectra were computed and compared to the experiment[35–37] for the three antiepileptic drugs, carbamazepine, lamotrigine, and diazepam. The first singlet ESA spectrum of [2,2]-paracyclophane (PCP) computed at the XsTDA/B3LYP level of theory is examined with respect to the EOM-EE-CCSD reference one from Krylov and coworkers.[38]

The XsTD-DFT/XsTDA methods inherit from all previous implementations in the `stda` program,[39] and thus, we also benchmark nonlinear optical properties. To assess the performance of the XsTD-DFT method to compute the first hyperpolarizability, six push-pull π-conjugated molecules were employed to assess the performance of the XsTD-DFT method. Finally for 2PA, we investigate the spectra for a set of fluorescent protein chromophores[40] and for eGFP with a model structure, including the chromophore and its first shell of surrounding residues.[41] Figure 3 shows these additional structures.

This paper is organized as follows: first, we introduce the theoretical background for the XsTD-DFT/XsTDA methods for global hybrid XC functionals, and then, we provide computational details and discuss results before providing conclusions and outlooks.

II. THEORETICAL BACKGROUND

The XsTD-DFT/XsTDA methods are introduced by first recalling the density-matrix-based TD-DFT formalism[8,42–47] and then showing how simplifications were originally applied to give rise to the sTD-DFT/sTDA framework[10,11,13,15–17,29] and finally how to remove its semi-empiricism. In the following, p, q, r, s indices refer to general molecular orbitals (MOs); i, j, k, l to occupied; a, b, c, d to unoccupied molecular orbitals; $\alpha, \beta, \gamma, \delta$ to atomic orbitals (AOs); and A and B to atoms. Casida's TD-DFT equations[5] are usually used to compute excited states,

$$\left[\begin{pmatrix}\mathbf{A} & \mathbf{B}\\ \mathbf{B} & \mathbf{A}\end{pmatrix} - \omega\begin{pmatrix}1 & 0\\ 0 & -1\end{pmatrix}\right]\begin{pmatrix}\mathbf{X}\\ \mathbf{Y}\end{pmatrix} = 0 \tag{1}$$

or linear response properties in the presence of a perturbation,

$$\left[\begin{pmatrix}\mathbf{A} & \mathbf{B}\\ \mathbf{B} & \mathbf{A}\end{pmatrix} - \omega\begin{pmatrix}1 & 0\\ 0 & -1\end{pmatrix}\right]\begin{pmatrix}\mathbf{X}_\zeta(\omega)\\ \mathbf{Y}_\zeta(\omega)\end{pmatrix} = -\begin{pmatrix}\mu_\zeta\\ \mu_\zeta\end{pmatrix}, \tag{2}$$

where X and Y are excitation and de-excitation vectors, respectively, $X_\zeta(\omega)$ and $Y_\zeta(\omega)$ are frequency-dependent linear-response vectors, and the perturbation is $\mu_{\zeta,ai} = \langle\phi_a|\hat{\mu}_\zeta|\phi_i\rangle$. For a hybrid exchange–correlation functional, **A** and **B** supermatrix elements are defined for a given amount a_x of Fock exchange as

$$\begin{aligned}A_{ia,jb} = {}& \delta_{ij}\delta_{ab}(\epsilon_a - \epsilon_i) + 2(ia|jb) - a_x(ij|ab)\\ & + (1 - a_x)(ia|f_{XC}|jb)\end{aligned} \tag{3}$$

and

$$B_{ia,jb} = 2(ia|bj) - a_x(ib|aj) + (1 - a_x)(ia|f_{XC}|bj), \tag{4}$$

where $(ia|jb)$, $(ia|bj)$, and $(ib|aj)$ are exchange-type integrals, $(ij|ab)$ are Coulomb-type two-electron integrals, and $(ia|f_{XC}|jb)$ and $(ia|f_{XC}|bj)$ are the response of the exchange–correlation functional. To compute excited states using the Tamm–Dancoff approximation, the **B** supermatrix is neglected, giving rise to a simple Hermitian eigenvalue problem,

$$\mathbf{AX} = \omega\mathbf{X}. \tag{5}$$

The sTD-DFT/sTDA framework applied three approximations to these equations. First, the terms involving the response of the exchange–correlation functional $(ia|f_{XC}|jb)$ and $(ia|f_{XC}|bj)$ are neglected in the expressions of **A** and **B** supermatrices. Second, the expansion space of configuration state functions (CSFs) is truncated considering a single cutoff energy E_{thresh}. In this procedure, the active MO space is determined for MO energies in between

$$\epsilon_{\min} = \epsilon_{LUMO} - 2(1 + 0.8a_x)E_{thresh} \tag{6}$$

and

$$\epsilon_{\max} = \epsilon_{HOMO} + 2(1 + 0.8a_x)E_{thresh}. \tag{7}$$

Then, the primary CSFs (P-CSFs) space is selected for $i \to a$ excitations when $A_{ia,ia} \le E_{thresh}$. Remaining $j \to b$ excitations for which $A_{jb,jb} > E_{thresh}$ are only selected as secondary CSF (S-CSF) if

$$E^{(2)}_{jb} = \sum_{ia}^{P-CSFs} \frac{|A_{ia,jb}|^2}{A_{jb,jb} - A_{ia,ia}} > 10^{-4}E_h. \tag{8}$$

The full space of CSFs accounted for in the sTD-DFT/sTDA procedures for a given E_{thresh} is the sum of P-CSFs and S-CSFs. The last approximation regards two-electron integrals that are approximated by a monopole approximation to balance the computational cost and accuracy. MO two-electron integrals should be normally evaluated by the four-index transformation of AO two-electron integrals,

$$(ia|jb) = \sum_{\alpha\beta\gamma\delta} C^*_{i\alpha}C_{a\beta}C^*_{j\gamma}C_{b\delta}(\alpha\beta|\gamma\delta). \tag{9}$$

This costly transformation can be a computational bottleneck in conventional "*ab initio*" quantum chemistry. Considering an orthogonalized Löwdin basis $\lambda_\alpha = \sum_\beta \chi_\beta S^{-1/2}_{\beta\alpha}$, MO two-electron integrals are equivalently computed as

$$(ia|jb) = \sum_{\alpha\beta\gamma\delta} C^{low*}_{i\alpha}C^{low}_{a\beta}C^{low*}_{j\gamma}C^{low}_{b\delta}(\lambda_\alpha\lambda_\beta|\lambda_\gamma\lambda_\delta). \tag{10}$$

Considering the ZDO approximation,[33] MO two-electron integrals are approximated as

$$(ia|jb) \approx \sum_{\alpha\beta} C^{low*}_{i\alpha}C^{low}_{a\alpha}C^{low*}_{j\beta}C^{low}_{b\beta}(\lambda_\alpha\lambda_\alpha|\lambda_\beta\lambda_\beta). \tag{11}$$

Assuming that Löwdin-orthogonalized orbitals (LOs) are atom-centered and, thus that the Löwdin-orthogonalized coefficients do

29 May 2024 06:59:37

Published under an exclusive license by AIP Publishing

belong to a particular atom, transition charges can be collected for atom A as

$$Q_A^{ia} = \sum_{\alpha \in A} C_{\alpha i}^{low*} C_{\alpha a}^{low}. \tag{12}$$

The simplified expression for MO two-electron integrals reads

$$(ia|jb) \approx \sum_{AB} Q_A^{ia} Q_B^{jb} (AA|BB), \tag{13}$$

where

$$(AA|BB) = \sum_{\alpha \in A, \beta \in B} (\lambda_\alpha \lambda_\alpha | \lambda_\beta \lambda_\beta). \tag{14}$$

This expression implies that Löwdin-orthogonalized two-electron integrals are available for atoms A and B. Equation (13) presents a simple Coulomb law where $(AA|BB)$ is approximated by the MNOK[30–32] damped Coulomb operator that does not depend on LOs λ_α anymore.

For exchange integrals, it takes the form,

$$(AA|BB)^K = \left(\frac{1}{(R_{AB})^{y_K} + \left(\frac{\eta_A + \eta_B}{2}\right)^{-y_K}} \right)^{\frac{1}{y_K}}, \tag{15}$$

while for Coulomb integrals, it reads

$$a_x (AA|BB)^J = \left(\frac{1}{(R_{AB})^{y_J} + \left(a_x \frac{\eta_A + \eta_B}{2}\right)^{-y_J}} \right)^{\frac{1}{y_J}}, \tag{16}$$

where y_K and y_J are globally fitted parameters for the whole range of a_x, R_{AB} is the interatomic distance, and η_A is the chemical hardness of atom A. This also means that the onsite integral $(AA|AA)$ is simply the chemical hardness η_A of A multiplied by a_x considering the type of integrals. The MNOK approximation eliminates the dependence on LOs of Eq. (14). These expressions are quite beneficial in terms of computational cost by first pre-computing

$$(ia|BB) = \sum_A Q_A^{ia} (AA|BB) \tag{17}$$

and then taking the dot product that only scales with the number of atoms when constructing **A** and **B** supermatrices,

$$(ia|jb) \approx \sum_B (ia|BB) Q_B^{jb}. \tag{18}$$

This constitutes the basis of the sTD-DFT/sTDA schemes.

Now, we introduce the XsTD-DFT/XsTDA methods. It is common in semi-empirical molecular orbital models[48] to replace Löwdin-orthogonalized two-electron integrals by AO ones according to

$$(ia|jb) \approx \sum_{\alpha\beta} C_{i\alpha}^{low*} C_{a\alpha}^{low} C_{j\beta}^{low*} C_{b\beta}^{low} (\alpha\alpha|\beta\beta). \tag{19}$$

Thus, AO transition charges can be collected for each basis functions as

$$Q_\alpha^{ia} = \sum_\alpha C_{\alpha i}^{low*} C_{\alpha a}^{low}. \tag{20}$$

Expression (19) becomes

$$(ia|jb) \approx \sum_{\alpha\beta} Q_\alpha^{ia} Q_\beta^{jb} (\alpha\alpha|\beta\beta). \tag{21}$$

In the same way as in sTD-DFT/sTDA schemes, its evaluation becomes computationally efficient by pre-computing

$$(ia|\beta\beta) = \sum_\alpha Q_\alpha^{ia} (\alpha\alpha|\beta\beta) \tag{22}$$

and then taking the dot product that scales with the number of AOs,

$$(ia|jb) \approx \sum_\beta (ia|\beta\beta) Q_\beta^{jb}. \tag{23}$$

In XsTD-DFT/XsTDA, we still consider the original three simplifications of the sTD-DFT method, but two-electron integrals to generate **A** and **B** supermatrices are now computed using one- and two-center AO two-electron integrals with Eq. (23). Thus, we removed part of the semiempirical nature of the sTD-DFT/sTDA methods.

Note that in our implementation, the CSFs space is still determined with the MNOK integrals for efficiency without any noticeable changes in the results. Compared to the sTD-DFT, XsTD-DFT is computationally more involved because the construction of the **A** and **B** supermatrices scales with the number of AOs rather than the number of atoms. Figure 4 shows the computation wall times as a function of the number of basis functions to compute the 20 first excited states for the benchmark set of 77 molecules (Figs. 1 and 2) at the B3LYP/6-31+G(d) level of theory on 8 CPUs (Intel Xeon CPU E5-2660 v4, 3.2 GHz). Wall times are also reported for the sB3LYP and XsB3LYP calculations considering

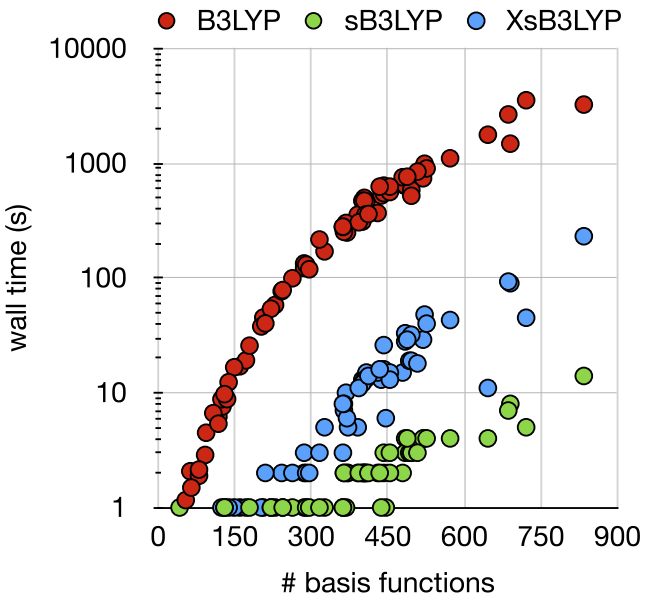


FIG. 4. B3LYP, sB3LYP, and XsB3LYP computation wall times as a function of the number of basis functions for the set of 77 molecules. TDA calculations computed 20 excited states, while sTDA and XsTDA ones considered $E_{thresh.} = 10$ eV.

29 May 2024 06:59:37

Published under an exclusive license by AIP Publishing

$E_{thresh.}$ = 10 eV performed on an 8 core desktop computer (Intel core i7-6700, 3.4 GHz) with Q-Chem 5.1.[49] Typically for $E_{thresh.}$ = 10 eV, more than 1000 excited states are computed for these systems. Note that the number of excited states computed depends on the system and $E_{thresh.}$, and thus, it is not possible to give formal scaling factors for simplified methods. As an example, for molecule **50**, 1204 and 1121 states were computed at sB3LYP and XsB3LYP levels of theory in 14 s and 3.85 min, respectively, while the full TD-DFT calculation took 26.5 min to compute 20 states. Using a smaller $E_{thresh.}$ value of 7 eV (`stda` program[39] default), the XsTDA calculation computed "only" 223 excited states in 23 s. This is more than 60 time faster with respect to the full scheme. For compound **35**, the TDA calculation took 25.5 min, while sTDA and XsTDA at $E_{thresh.}$ = 10 eV only took 4 and 11 s, respectively, corresponding to a speed-up of 382 and 139, respectively. For this benchmark set and $E_{thresh.}$ = 10 eV, the average speed-up is around 100 for sTDA and 20 for XsTDA. These factors can be increased by using a smaller $E_{thresh.}$ value.

III. COMPUTATIONAL DETAILS

The XsTD-DFT/XsTDA methods were implemented in a development version of the freely available `stda` program,[39] which is now interfaced with the Libcint library[50] to enable the computation of two-electron AO integrals. This implementation benefits from the whole range of linear and nonlinear optical properties already implemented at the sTD-DFT/sTDA levels of theory in the `stda` program,[39] including UV–vis absorption,[10,11] CD,[10,11] polarizability,[15] optical rotation,[16] ESA,[17] first hyperpolarizability,[15] and two-photon absorption.[18]

To test the performance of the XsTDA method to compute excited state energies and oscillator strengths, geometries of 77 molecules (Figs. 1 and 2) were taken from previous studies.[11–13,34] For **10** and **47–57**, back-corrected "experimental" vertical excitation energies are taken from Ref. 34. Molecules **69–77** are parts of the mixed CT test set[12] for which reference excitation energies for transitions to CT states are available at the SCS-CC2/def2-TZVP(-f) level of theory. Additional RI-CC2/aug-cc-pVDZ excitation energies were computed for **72** for different distances between benzene and TCNE molecular plans.

To assess the performance of the XsTDA method to compute UV–vis absorption spectra, we first compare it to the experimental spectrum of the largest molecule of the benchmark set of 77 molecules, i.e., molecule **50** (perylene-3,4,9,10-tetracarboxylic bisimide) that was taken from Langhals.[51] Second, the structure of ferrocene was optimized at the ωB97X-D3/def2-TZVP level of theory. Its experimental absorption spectrum was taken from Ref. 10 for comparison. Third, we selected the three drugs, carbamazepine, lamotrigine, and diazepam, the structures of which were optimized at the ωB97X-D3/6-311G(d) level of theory. The experimental UV–vis absorption spectra were taken from Refs. 35–37, respectively. PCP geometry and the reference EOM-EE-CCSD ESA spectrum were taken from Ref. 38.

The reference TD-DFT/TDA excited state calculations were performed with Q-CHEM[49] using B3LYP, PBE0, BHandHLYP, and M06-2X functionals and the 6-31+G(d) basis set for the set of 77 molecules. BHandHLYP/6-31+G(d) TD-DFT/TDA calculations were also performed with Q-CHEM[49] for carbamazepine, lamotrigine, and diazepam, while sTDA and XsTDA computations employed the same functional/basis set combination. For the set of 77 molecules, an energy threshold of 10 eV was employed to truncate the CSFs space, while the default value of 7 eV was used for other compounds. For ferrocene, the 20 first excited states were computed at the PBE0/def2-TZVP/TD-DFT/TDA level of theory and compared to the sTDA and XsTDA results using $E_{thresh.}$ = 7 eV. Note that to simulate intensity borrowing by vibronic coupling, forbidden transition oscillator strengths were set to 5×10^{-4} as it was originally proposed by one of us.[10]

To assess the performance of the XsTD-DFT method to reproduce frequency-dependent hyper-Rayleigh scattering first hyperpolarizability (β_{HRS}) values, the structures of six push-pull π-conjugated molecules, which were originally used to benchmark the sTD-DFT method,[15] were taken from de Wergifosse and Champagne.[41] TD-DFT and sTD-DFT BHandHLYP/6-31+G(d) β_{HRS} frequency dispersions were taken from our previous study de Wergifosse and Grimme[15] The XsTD-DFT β_{HRS} values were computed at the same level.

For 2PA, we first used the same set of FP chromophores that we employed to benchmark the sTD-DFT method.[18] These structures were taken from Ref. 40 and reference excitation energies as well as 2PA cross sections (σ_{2PA}) at the RI-CC2/d-aug(-d)-cc-pVDZ level for HBI, HBDI, and PYP and with the aug-cc-pVDZ basis set for CFP as well as EOM-CCSD/d-aug(-d)-cc-pVDZ level,[52] when available. Second, we took eGFP chromophore and its first shell of surrounding residues from de Wergifosse *et al.*[53] This structure was successfully used to evaluate the 2PA spectrum of eGFP at the sTD-DFT-xTB level of theory.[18] The experimental 2PA spectrum was recorded by Drobizhev *et al.*[54] Regarding FP chromophores, TD-DFT 2PA cross sections and excited state energies were computed using Dalton2018.0[55,56] with the 6-31+G(d) basis set and B3LYP. The sTD-DFT and XsTD-DFT calculations were performed with the same XC functionals and basis set. For eGFP, the B3LYP/6-31G(d) calculations were performed at both the sTD-DFT and XsTD-DFT levels of theory.

Input molecular orbitals and their energies for the sTD-DFT and XsTD-DFT calculations used by the `stda` program[39] were computed with Q-Chem 5.1.[49] All geometry optimizations were also performed with Q-Chem.[49] RI-CC2 excitation energies were computed with Turbomole 7.6.[57] The β_{HRS} values are given in atomic units considering the Taylor series convention,[58] while 2PA strengths $\langle \delta^{2PA} \rangle$ are in a.u. and σ_{2PA} in GM (Göppert–Mayer) units.

IV. RESULTS AND DISCUSSIONS

A. Excitation energies, oscillator strengths, and UV–vis spectra

Figure 5 shows the excitation energy and oscillator strength correlation plots for the two lowest-lying singlet excited states of the set of 77 molecules for sTDA and XsTDA with respect to TDA using B3LYP, PBE0, BHandHLYP, and M06-2X XC functionals. For each functional, Table I presents statistical analysis of the excitation energies and oscillator strengths considering regular TDA results as the reference. For oscillator strengths, statistical analysis are given by orders of magnitude ($f \in [0.0; 0.1[$, $[0.1; 1.0[$, and $[1.0; 3.0]$). Note that the first range of magnitude includes the order from 0.01 to 0.1 but

29 May 2024 06:59:37

Published under an exclusive license by AIP Publishing

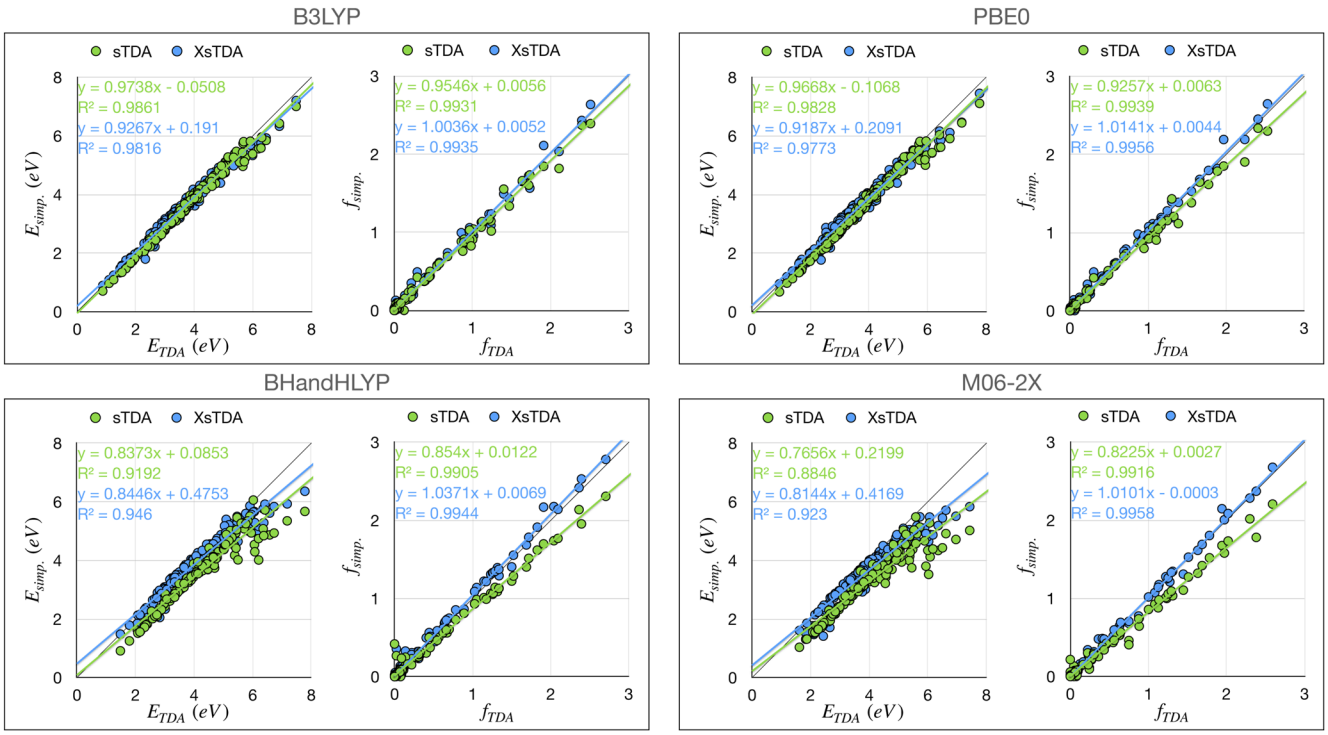


FIG. 5. For the two lowest-lying singlet excited states of the set of 77 molecules, correlation graphs for sTDA and XsTDA excitation energies with respect to TDA ones as well as for oscillator strengths using B3LYP, PBE0, BHandHLYP, and M06-2X exchange–correlation functionals and the 6-31+G(d) basis set. Linear regression data are also provided.

TABLE I. For B3LYP, PBE0, BHandHLYP, and M06-2X exchange–correlation functionals, mean absolute deviations (MAD), difference between maximum and minimum absolute deviations (AD), and mean deviations (MD) among the set of 77 molecules for sTDA and XsTDA excitation energies and oscillator strengths with respect to TDA ones. The sign of MD indicates a systematic overestimation or underestimation.

E (eV)	sB3LYP	XsB3LYP	sPBE0	XsPBE0	sBHandHLYP	XsBHandHLYP	sM06-2X	XsM06-2X
MAD	0.16	0.14	0.24	0.16	0.61	0.24	0.74	0.35
max AD - min AD	0.70	0.70	0.92	0.74	2.18	1.42	2.45	1.60
MD	−0.15	−0.08	−0.24	−0.10	−0.60	−0.18	−0.74	−0.35
f ∈ [0.0; 0.1[	sB3LYP	XsB3LYP	sPBE0	XsPBE0	sBHandHLYP	XsBHandHLYP	sM06-2X	XsM06-2X
MAD	0.01	0.01	0.01	0.01	0.01	0.01	0.01	0.01
max AD - min AD	0.06	0.11	−0.05	−0.08	0.42	0.33	0.22	0.07
MD	+0.00	+0.00	+0.00	+0.00	+0.01	+0.00	+0.00	0.00
f ∈ [0.1; 1.0[	sB3LYP	XsB3LYP	sPBE0	XsPBE0	sBHandHLYP	XsBHandHLYP	sM06-2X	XsM06-2X
MAD	0.04	0.05	0.03	0.04	0.05	0.05	0.10	0.06
max AD - min AD	0.15	0.19	0.15	0.19	0.11	0.19	0.34	0.14
MD	−0.01	+0.02	−0.01	+0.03	+0.07	+0.03	−0.09	−0.00
f ∈ [1.0; 3.0]	sB3LYP	XsB3LYP	sPBE0	XsPBE0	sBHandHLYP	XsBHandHLYP	sM06-2X	XsM06-2X
MAD	0.09	0.06	0.12	0.05	0.22	0.08	0.27	0.04
max AD - min AD	0.29	0.20	0.33	0.22	0.37	0.26	0.46	0.20
MD	−0.07	−0.00	−0.11	+0.02	−0.22	+0.07	−0.27	+0.02

29 May 2024 06:59:37

Published under an exclusive license by AIP Publishing

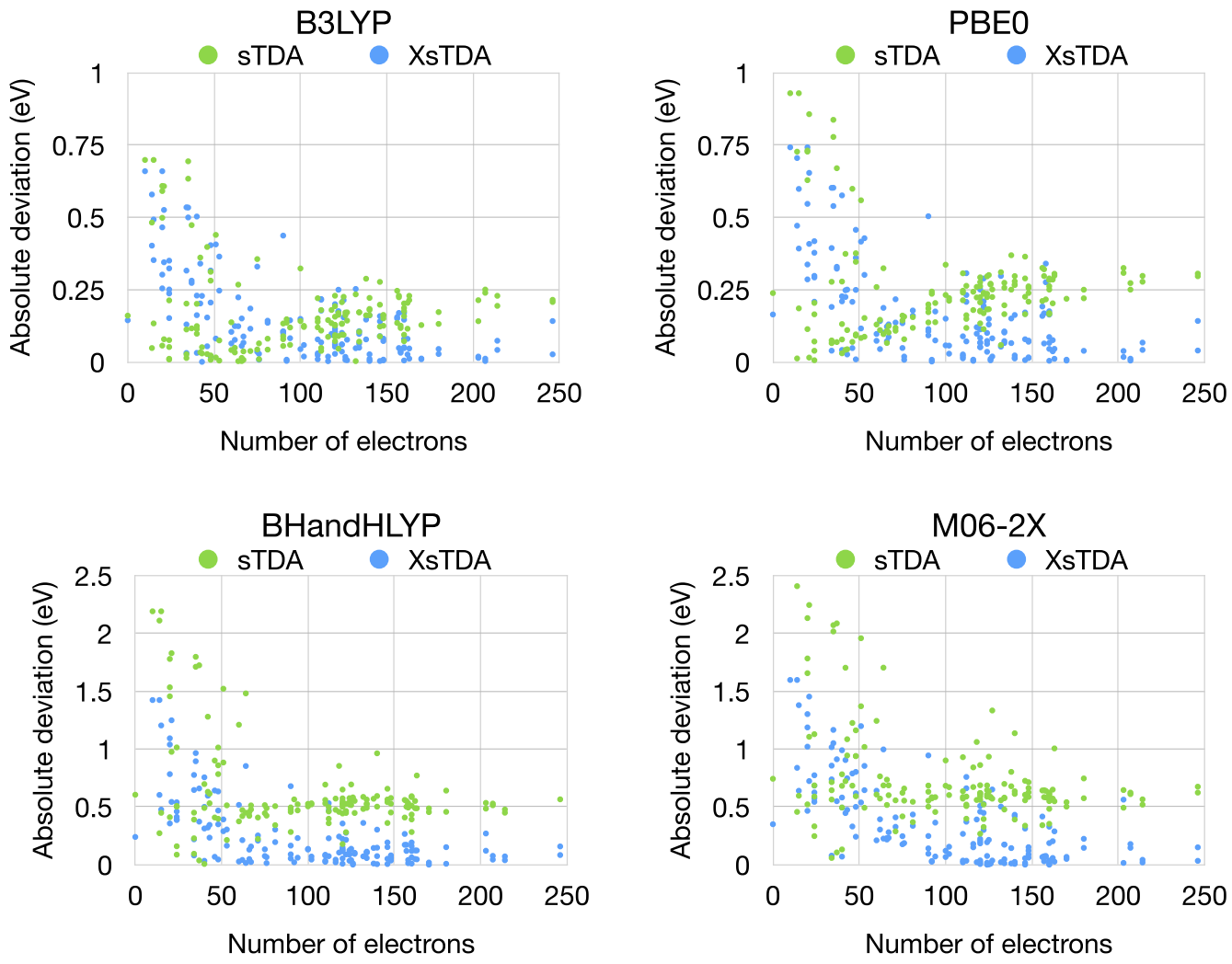


FIG. 6. Excitation energy absolute deviations of both sTDA and XsTDA methods with respect to TDA calculations as a function of the number of electrons for B3LYP, PBE0, BHandHLYP, and M06-2X functionals for the set of 77 molecules.

also lower oscillator strengths for convenience. The statistical analysis includes mean absolute deviations (MAD), differences between maximum and minimum absolute deviations (AD) representing the error spread, and mean deviations (MD) for which the sign indicates systematic overestimation or underestimation.

For B3LYP, both sTDA and XsTDA excitation energies deviate only slightly with respect to TDA ones with MAD values of 0.16 and 0.14 eV for sTDA and XsTDA, respectively. This shows that the sTDA method is particularly well parameterized for small amounts of Fock exchange as in B3LYP. The error spreads have

TABLE II. Excitation energies (eV), oscillator strengths, and types of transition for the two lowest-lying singlet excited states of uracil obtained with BHandHLYP/6-31+G(d) TDA, sTDA, and XsTDA schemes.

	TDA			sTDA			XsTDA		
Uracil	ΔE (eV)	f	Transition	ΔE (eV)	f	Transition	ΔE (eV)	f	Transition
1	5.38	0.00	$n \rightarrow \pi^*$	4.52	0.00	$\pi \rightarrow Ry$	5.03	0.00	$n \rightarrow \pi^*$
2	5.91	0.29	$\pi \rightarrow \pi^*$	5.19	0.00	$n \rightarrow \pi^*$	5.36	0.01	$\pi \rightarrow Ry$
3				5.40	0.00	$\pi \rightarrow Ry$	5.86	0.32	$\pi \rightarrow \pi^*$
4				5.51	0.24	$\pi \rightarrow \pi^*$			

29 May 2024 06:59:37

Published under an exclusive license by AIP Publishing

the same order of magnitude for both methods. Oscillator strength MADs are small for their respective ranges of magnitude with both the methods. The XsB3LYP scheme slightly outperforms sB3LYP for oscillator strengths larger or equal to 1.0 with respect to the B3LYP results, as clearly shown in the correlation graph (Fig. 5).

Considering PBE0 with 25% Fock exchange, the MAD is increased to 0.24 eV for sTDA, while it remains almost constant for XsTDA with 0.16 eV. Increasing the amount of Fock exchange in the functional globally increases the MAD for the sTDA scheme as confirmed by the sBHandHLYP and sM06-2X results. Excitation energy deviations remain smaller with XsTDA than for sTDA. The sM06-2X MAD of 0.74 eV is more than two times larger than the XsM06-2X MAD of 0.35 eV. Similar trends are observed for oscillator strengths especially in the [1.0; 3.0] range for which the XsTDA method clearly outperforms sTDA (Fig. 5). Perylene (**9**) was one of the sTDA "outliers" pointed out by one of us[10] with an absolute energy deviation larger than 0.50 eV at the sPBE0/TZVP level with respect to the experiment. For its first low-lying excited state, the TDA/PBE0/6-31+G(d) excitation energy is 0.37 eV smaller than the experimental value of 3.44 eV, while the XsPBE0 value deviates by only −0.27 eV. This is a significant improvement with respect to the sTDA absolute deviation of 0.60 eV.

Figure 6 presents the sTDA and XsTDA excitation energy absolute deviations (ADs) with respect to regular TDA as a function of the number of electrons in the molecule. Considering all four functionals, ADs are diminishing with increasing number of electrons for both sTDA and XsTDA with respect to TDA. ADs are globally lower for large systems when using the XsTDA method rather than the sTDA one. This supports the suitability of the XsTDA scheme to compute excitation energies for low-lying excited states of large systems.

For the DYE12 benchmark set, Tables S1 and S2 compare the computed sTDA and XsTDA excitation energies to TDA as well as to the back-corrected experiment. The XsTDA method reproduced TDA excitation energies well with MADs of about 0.10 eV. With respect to the back-corrected experiment, the best result is provided by the XsB3LYP scheme with a MAD of 0.23 eV, while TDA yields a value of 0.24 eV. Note that the best sTDA comparison with respect to the experiment is obtained with the BHandHLYP functional with a MAD of 0.23 eV. Clearly, the sTDA parametrization and error cancellations play a role here, as indicated by the TDA MAD of 0.37 eV with respect to the experiment.

As originally pointed out by one of us,[10] while $\pi \rightarrow \pi^*$ transitions are relatively well-treated by sTDA, larger discrepancies are expected for $n \rightarrow \pi^*$ and $d \rightarrow d$ transitions due to the applied monopole approximation, which fails for such cases. To illustrate this behavior and how the XsTDA scheme deals with these types of excitations, we first selected uracil (**4**) that presents a dipole-forbidden $n \rightarrow \pi^*$ excitation and a $\pi \rightarrow \pi^*$ transition as the two first low-lying singlet excited states. Table II presents the excited state energies and oscillator strengths, as obtained by the BHandHLYP/6-31+G(d) TDA, sTDA, and XsTDA schemes. First, both sTDA and XsTDA schemes yield $\pi \rightarrow Ry$ unwanted low-lying "ghost" states that are not present in the TDA calculation. Second, the $\pi \rightarrow \pi^*$ transition is better treated by the XsTDA method with only −0.05 eV of deviation with respect to the full scheme, while the sTDA error is −0.40 eV. For, the $n \rightarrow \pi^*$ transition, relatively large deviations are observed with both sTDA and XsTDA schemes (−0.19 and −0.35 eV). As stressed by one of us,[10] $n \rightarrow \pi^*$ transition are badly described by sTD-DFT/sTDA because of wrong localized exchange-type contributions due to the monopole approximation. This is inherent to any ZDO-based methods, such as the XsTD-DFT/XsTDA formalism, since one-center exchange integrals $[(\alpha\beta|\alpha\beta)$, α and $\beta \in A]$ are excluded.[59] Thus, the XsTD-DFT/XsTDA formalism presents the same problem as the sTD-DFT/sTDA scheme to describe local $n \rightarrow \pi^*$ transitions. A possible correction could be to use the INDO (intermediate neglect of differential overlap) approximation[60] instead of the ZDO one.

As a second illustrative case, we selected the ferrocene molecule that was already used in the original sTDA publication[10] to illustrate the relative poor treatment of $d \rightarrow d$ transitions by the sTDA method. Figure 7 shows the experimental absorption spectrum of ferrocene in comparison with the PBE0/def2-TZVP TDA, sTDA, and XsTDA spectra. The experimental spectrum presents three main absorption bands where the two lowest ones are related to dipole-forbidden metal-centered $d \rightarrow d$ transitions. These two bands are poorly described by the sTDA method, which are significantly improved with the XsTDA scheme. The rest of the XsTDA spectrum is globally blueshifted with respect to the experiment.

Treating electronic transitions to Rydberg states correctly is probably out of the scope of XsTD-DFT/XsTDA schemes. Nevertheless, among the test set, we have the first one photon-active transition $n \rightarrow Ry(3s)$ of acetone (**3**) with an experimental excitation energy of 6.35 eV and a reference theoretical oscillator strength of 0.037 (MRCI[1]). At the B3LYP/6-31+G(d) level, the experimental excitation energy is largely overestimated with a value of 6.91 eV, but the

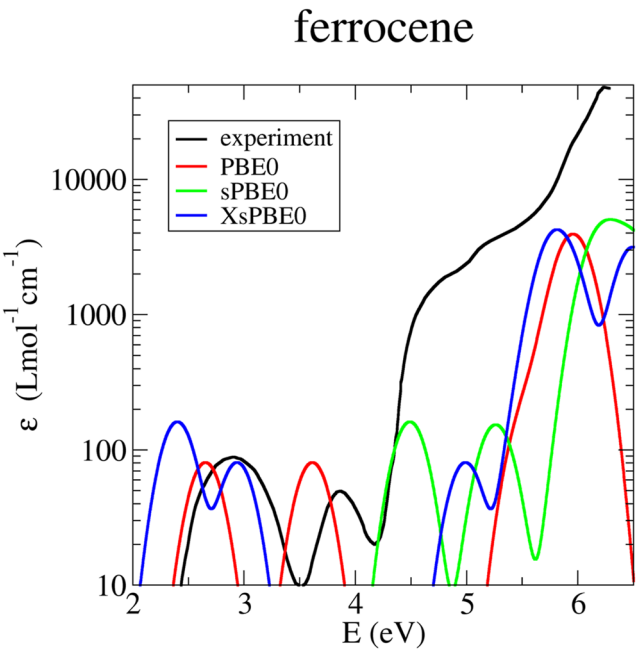


FIG. 7. Experimental absorption spectrum of ferrocene in comparison with the PBE0/def2-TZVP TDA, sTDA, and XsTDA spectra. Note that the oscillator strengths for forbidden transitions are set to 5×10^{-4} to simulate vibronic couplings.

29 May 2024 06:59:37

Published under an exclusive license by AIP Publishing

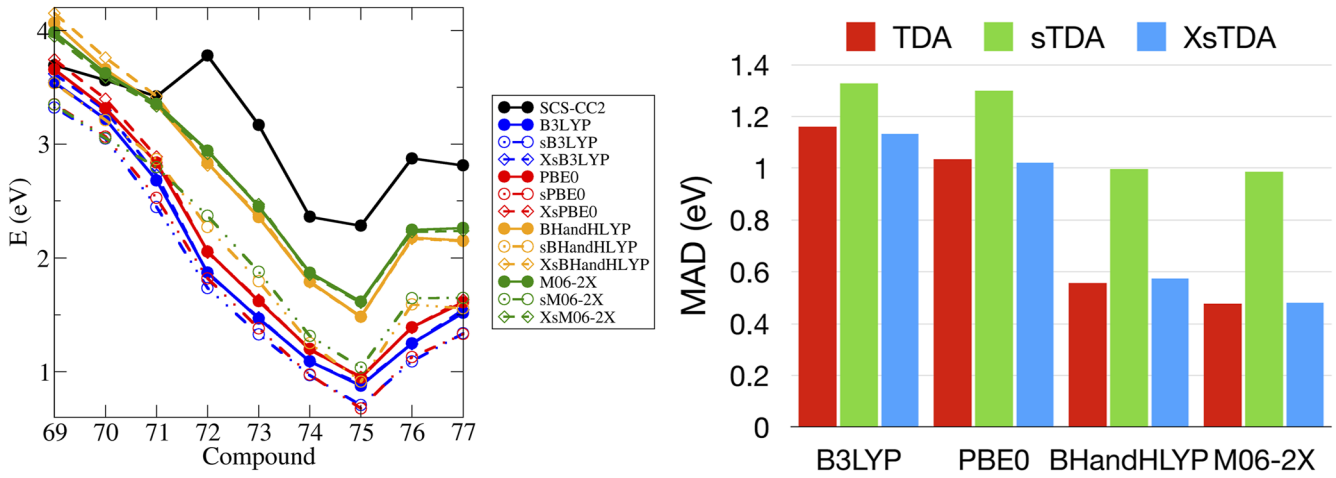


FIG. 8. Excitation energies (left panel) computed at TDA, sTDA, and XsTDA levels using B3LYP, PBE0, BHandHLYP, and M06-2X exchange–correlation functionals and the 6-31+G(d) basis set in comparison with reference SCS-CC2/def2-TZVP(-f) values for the mixed CT test set.[12] The mean absolute deviations (right panel) for all these levels of theory with respect to SCS-CC2.

MRCI oscillator strength is well reproduced with a value of 0.035. Only one pair of natural transition orbitals (NTOs) contributes to this transition, confirming its $n \rightarrow Ry(3s)$ character (see Fig. S2). The treatment is surprisingly improved with the XsB3LYP scheme giving an excitation energy of 6.33 eV and $f = 0.037$. The shape of NTOs at this level are similar to B3LYP ones. The sB3LYP level of theory is also providing a better energy value with respect to the full scheme with 6.46 eV ($f = 0.035$).

Hybrid XC functionals do not provide a good description for electron transitions to CT states. Usually, increasing the amount of Fock exchange in the functionals improves the treatment, but still large deviations are observed.[10,61] Employing RSH functionals is the usual solution for a better treatment of CT states but is not yet implemented with XsTD-DFT/XsTDA schemes. To assess the performance of the XsTDA scheme to treat CT states, the mixed CT test set from Risthaus *et al.*[12] was taken. Figure 8 shows the comparison between the TDA, sTDA, and XsTDA excitation energies to CT states using B3LYP, PBE0, BHandHLYP, and M06-2X exchange–correlation functionals and 6-31+G(d) basis set and reference SCS-CC2/def2-TZVP(-f) values. MADs for these excitation energies with respect to SCS-CC2 are also reported. As expected, the XC functional with a large amount of HF exchange agrees best with the reference. MADs for BHandHLYP and M06-2X are 0.56 and 0.48 eV, respectively. XsTDA reproduces the TDA results almost perfectly, while sTDA on the contrary presents larger MADs of 1.0 eV (sBHandHLYP) and 0.98 eV, respectively. Regarding intermolecular CT states for systems **72–77**, all reference excitation energies are systematically underestimated by TDA, a behavior almost perfectly reproduced by the XsTDA scheme.

Molecule **72** is composed of one benzene unit and one TCNE unit, for which their molecular planes are parallel to each other. Figure 9 shows the first low-lying excited state energy of this system shown in the inset of Fig. 9 for NTOs as a function of the distance (R) between both molecular planes evaluated at the TDA, sTDA, and XsTDA [BHandHLYP/6-31+G(d)] levels of theory with respect to the reference RI-CC2/aug-cc-pVDZ. A reference curve is also provided and computed as $E_{CT} = IP' - EA' - 1/R$, where IP' refers to the KS-DFT HOMO energy of benzene and EA', the KS-DFT LUMO energy of TCNE. All TDA, sTDA, and XsTDA

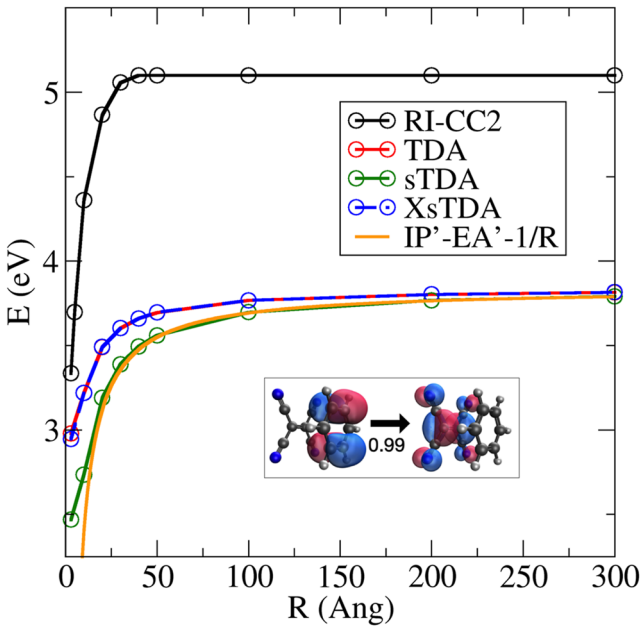


FIG. 9. Comparison of CT excitation energies computed at TDA, sTDA, and XsTDA [BHandHLYP/6-31+G(d)] levels of theory with respect to the RI-CC2/aug-cc-pVDZ reference for molecule **72** as a function of the distance (R) between both parallel molecular plan of benzene and TCNE. A reference analytical single-particle curve is also provided. The inset presents the natural transition orbitals obtained at the TDA/BHandHLYP/6-31+G(d) level of theory for the first low-lying state. Only one pair contributes to the transition with a weight of 0.99.

29 May 2024 06:59:37

Published under an exclusive license by AIP Publishing

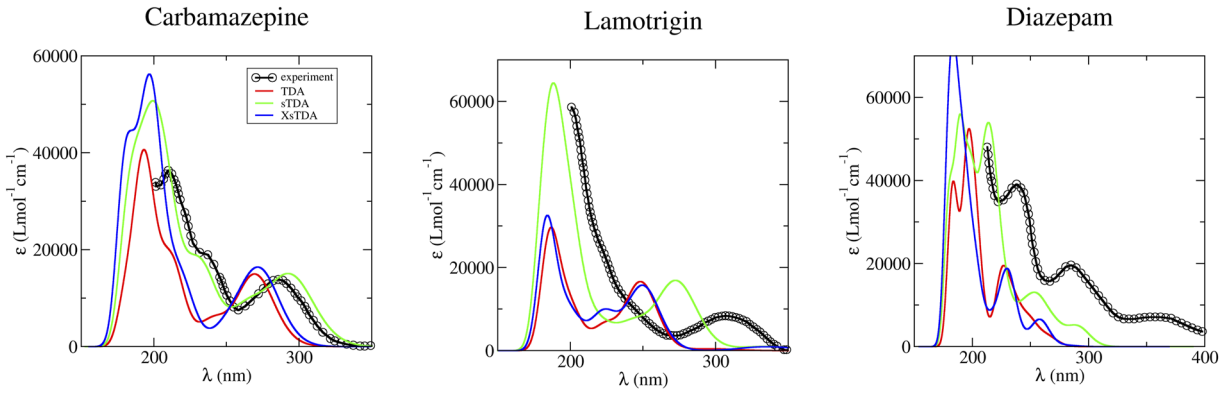


FIG. 10. UV–vis experimental absorption spectra[35–37] of carbamazepine in methanol, lamotrigine, and diazepam in water as well as BHandHLYP/6-31+G(d) TDA, sTDA, and XsTDA spectra in vacuum.

results asymptotically tend to an excitation energy value of around 1.3 eV lower than the RI-CC2 one. This is expected for hybrid XC functionals because of the integer discontinuity problem and the self-interaction error.[10,62–64] At large distance, this CT state is composed of benzene$^+$ and TCNE$^-$, two charges with a $1/R$ interaction energy. In TD-DFT, this interaction is described by the $-(ii|aa)$ term in Eq. (1) but scaled inappropriately by a_x, hence not providing the expected $1/R$ decay. By design, the sTDA scheme was corrected for this behavior by asymptotically approaching the $1/R$ contribution directly into the semi-empirical integral [see Eq. (16)].[10] This is illustrated in Fig. 9 showing that the sTDA scheme reproduces the $E_{CT} = IP' - EA' - 1/R$ curve well, while the XsTDA scheme matches almost perfectly with the TDA results.

Figure 10 shows the experimental absorption spectra[35–37] of three anti-epileptic drugs, carbamazepine, lamotrigine, and diazepam, recorded in methanol for the carbamazepine and in water for lamotrigine and diazepam. They are compared to the BHandHLYP/6-31+G(d) TDA, sTDA, and XsTDA vertical spectra.

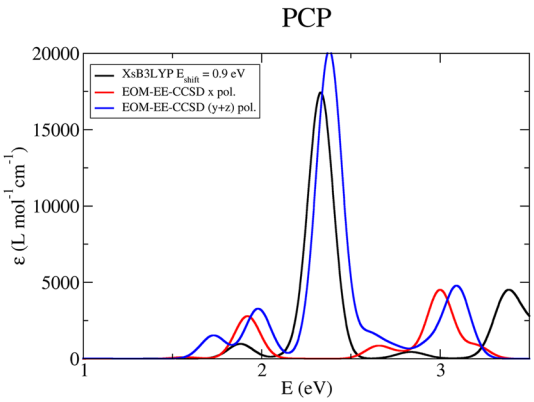


FIG. 11. Comparison of the first singlet ESA spectrum for PCP computed at XsB3LYP/TDA/6–311++G(d,p) to reference the EOM-EE-CCSD/6–311++G(d,p) spectra for both x and $(y + z)$ polarizations. An energy shift of 0.9 eV was applied to the XsB3LYP spectrum.

As it was observed for the benchmark set, sBHandHLYP/TDA excitation energies are redshifted with respect to the BHandHLYP/TDA ones, which is corrected by XsTDA and the TDA spectra are well reproduced. However, both the TDA and XsTDA spectra are systematically blueshifted with respect to the experiment because of a missing solvent, relaxation, and vibrational effects.

PCP is a model for studying benzene excimer. Figure 11 shows its first singlet ESA spectra computed at both EOM-EE-CCSD and XsB3LYP levels of theory. The XsB3LYP reproduces well the intensity of the main absorption band around 2.38 eV with respect to the EOM-EE-CCSD one. As it could be expected using the B3LYP XC functional, some features of the reference spectrum are not present, such as some lower energy peaks below 2 eV. Nevertheless, the comparison is rather good for such low-level treatment.

B. Second-harmonic generation of push-pull π-conjugated systems

One recurring problem with the sTD-DFT scheme to evaluate β_{HRS} is the systematically redshifted resonance enhancements with respect to the full scheme for push-pull π-conjugated molecules. To circumvent this, we advocated refitting the MNOK two-electron integral parameters.[15,29,65]

Figure 12 shows the β_{HRS} frequency dispersions obtained at BHandHLYP/6-31+G(d) TD-DFT, sTD-DFT, and XsTD-DFT levels of theory for six push-pull π-conjugated molecules. The XsTD-DFT method reproduces TD-DFT β_{HRS} frequency dispersions almost perfectly and, in particular, the energy position of the resonance enhancement, clearly outperforming the sTD-DFT scheme. This is easily explainable as these resonance enhancements are due to the CT states for which XsTD-DFT is particularly good at reproducing the TD-DFT excitation energies. The computational cost to evaluate the first hyperpolarizability at the XsTD-DFT level is very low with respect to the full scheme. Computing one single β_{HRS} value for **m-3** with GAMESS[66,67] took 30.9 min[15] on an 8 cores desktop computer (Intel core i7-6700, 3.40 GHz), while the XsTD-DFT calculation finished in only 5.2 min for 13 β_{HRS} values. The sTD-DFT calculation took 1.9 min.

29 May 2024 06:59:37

Published under an exclusive license by AIP Publishing

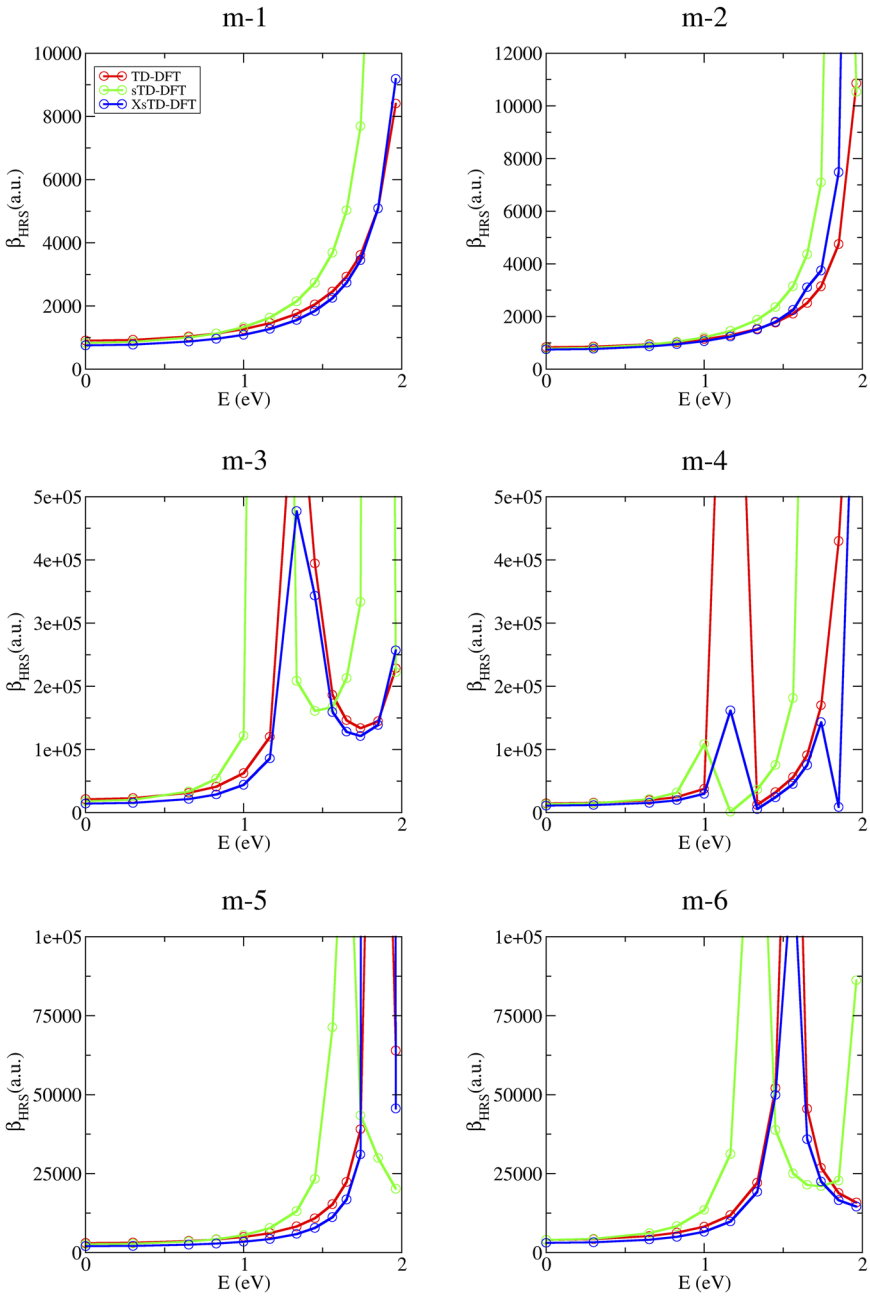


FIG. 12. β_{HRS} frequency dispersions obtained at BHandHLYP/6-31+G(d) TD-DFT, sTD-DFT, and XsTD-DFT levels of theory for the six push-pull π-conjugated molecules. For sTD-DFT and XsTD-DFT calculations, $E_{thresh.}$ = 15 eV was used.

C. Two-photon absorption

Recently, we showed that calculating absolute 2PA cross sections [depending on $(2\omega)^2$ and the half width at half maximum for a given line shape] is inherently difficult for TD-DFT and *de facto* for simplified methods based on TD-DFT.[18] The error for the excitation energy directly impacts the 2PA cross section. Regarding 2PA strengths [independent of $(2\omega_{ge})^2$] among a set of push-pull π-conjugated systems, Zaleśny and coworkers[68] demonstrated that global hybrid functionals are not well reproducing trends but have better absolute values, while RSH functionals underestimate

29 May 2024 06:59:37

Published under an exclusive license by AIP Publishing

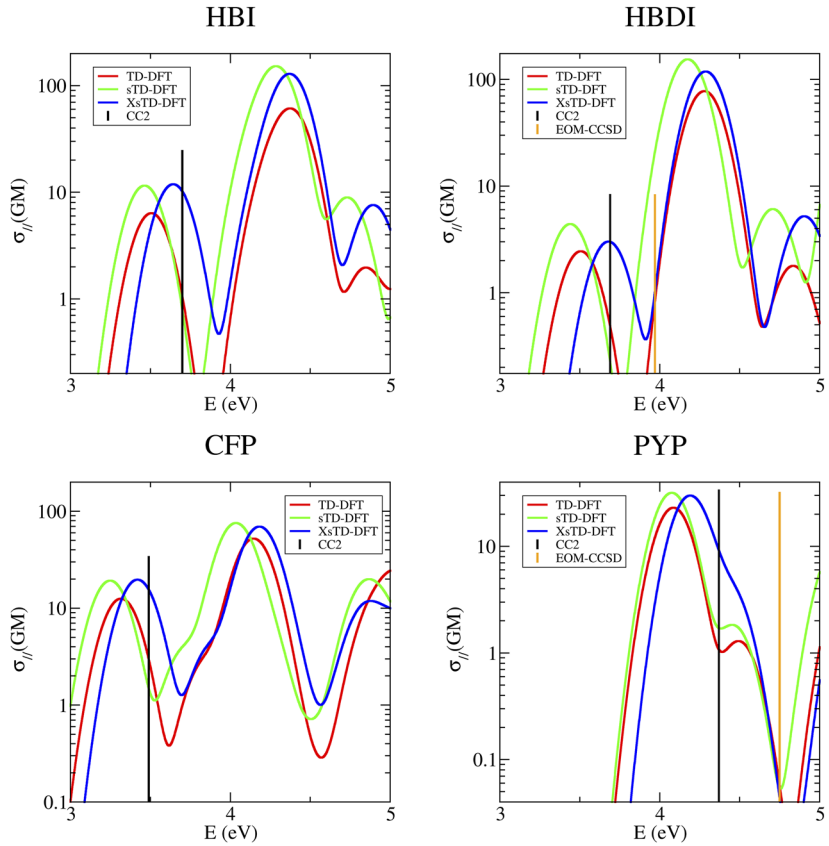


FIG. 13. 2PA spectra for HBI, HBDI, CFP, and PYP computed at B3LYP/6-31+G(d) TD-DFT, sTD-DFT, and XsTD-DFT in comparison to reference RI-CC2/d-aug(-d)-cc-pVDZ or aug-cc-pVDZ excitation energies and 2PA cross sections for the lowest energy excited state from Beerepoot *et al.*[40] and EOM-CCSD/d-aug(-d)-cc-pVDZ reference calculations from 52, when available.

RI-CC2 2PA strengths but better correlate with them. RSH functionals will be implemented soon at the XsTD-DFT level. Note that currently the XsTD-DFT method is extensively benchmarked for 2PA on the benchmark set from Zaleśny and coworkers[68] as well as on compounds from the QUEST database[69–71] at UCLouvain.

Figure 13 compare the B3LYP TD-DFT, sTD-DFT, and XsTD-DFT 2PA spectra to RI-CC2 and EOM-CCSD excitation energy and σ^{2PA} for the lowest excited state of the four FP chromophores HBI, HBDI, CFP, and PYP. E_{thresh} = 9 eV was employed for the simplified calculations, and a logarithmic scale was used to highlight small 2PA cross sections.

Figure S1 shows that 2PA spectra are almost identical using larger basis sets (aug-cc-pVDZ and d-aug-cc-pVDZ), and thus, the 6-31+G(d) basis set was selected. TD-DFT 2PA spectral shapes are globally well-reproduced by both simplified methods. The sTD-DFT 2PA spectra are slightly redshifted with respect to the TD-DFT ones, while XsTD-DFT excitation energies are blueshifted. Considering the first bright 2P-induced excitation energy for the four systems with respect to the RI-CC2 results, MAD of 0.22, 0.26, and 0.09 eV are obtained for TD-DFT, sTD-DFT, and XsTD-DFT, respectively. Comparing orders of magnitudes of 2PA strengths with respect to RI-CC2 ones, MADs for log σ^{2PA} are 0.34 (B3LYP), 0.18 (sB3LYP), and 0.24 (XsB3LYP). This shows that the XsB3LYP excitation energies are in very good agreement with the RI-CC2 ones, but 2PA strengths are slightly better reproduced by the sB3LYP scheme. Note that for the first bright 2PA excitation of HBDI and PYP, all the results are redshifted with respect to EOM-CCSD excitation energies.

Figure 14 shows the experimental 2PA spectrum recorded by Drobizhev *et al.*[54] as well as the 2PA B3LYP/6-31G(d) sTD-DFT and XsTD-DFT spectra obtained for an eGFP model system (the deprotonated chromophore and its first shell of surrounding residues with 359 atoms). This model system was successfully used to reproduce the experimental 2PA spectrum at the sTD-DFT-xTB level of theory.[18] Note that the XsB3LYP 2PA spectrum was globally redshifted by 0.60 eV. Both sB3LYP and XsB3LYP spectra compare very well with the experiment.

29 May 2024 06:59:37

Published under an exclusive license by AIP Publishing

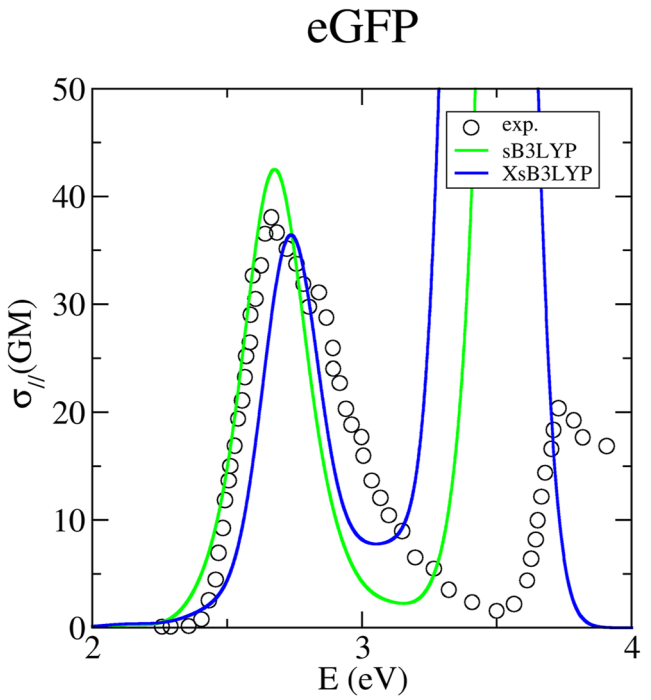


FIG. 14. Experimental 2PA spectrum from Drobizhev *et al.*[54] in comparison with the sB3LYP and XsB3LYP ones computed with the 6-31G(d) basis set, E_{thresh} = 7 eV and N = 2 [see Eq. (16) Ref. 18]. An energy shift of −0.60 eV was applied to the XsTD-DFT spectrum.

V. CONCLUSIONS

This contribution introduced XsTD-DFT, a computationally efficient method designed to calculate linear and nonlinear optical properties of large systems. It is based on the sTD-DFT scheme for which semi-empirical integrals are replaced by exact one- and two-center AO two-electron integrals. This new parameter-free method still uses the ZDO approximation with Löwdin-orthogonalized LCAO coefficients to compute MO two-electron integrals. This modification still keeps the XsTD-DFT method computationally efficient with respect to TD-DFT by drastically cutting computational costs by a factor of 20 or more depending on the single energy threshold used. The main difference appears in the construction of **A** and **B** TD-DFT supermatrices, where the XsTD-DFT method scales with the number of AOs instead of the number of atoms. Compared to sTD-DFT, these changes were implemented to robustly reproduce the TD-DFT results. A TDA variant named XsTDA was also implemented. Both schemes are currently limited to global hybrid XC functionals but can be extended to the RSH level.

The XsTDA scheme was tested for vertical excitation energies of a set of 77 molecules and compared to the conventional TDA results using B3LYP, PBE0, BHandHLYP, and M06-2X XC functionals. With respect to the previous sTDA scheme, XsTDA is more robust at reproducing TDA results especially when using XC functionals with large amount of Fock exchange. Oscillator strengths are also improved with XsTDA, especially for large f values. Interestingly, we observed that excitation energy absolute deviations decrease with increasing size of the system, a behavior most welcomed for a method designed to treat large systems. In 2013, one of us[10] showed that sTDA performs badly when computing $n \rightarrow \pi^*$ and metal-centered $d \rightarrow d$ transitions. The treatment of $n \rightarrow \pi^*$ transitions is not much improved by the XsTDA scheme because of the inherent ZDO approximation that neglects one-center exchange integrals. An INDO treatment might solve this problem. Regarding $d \rightarrow d$ transitions, the XsTDA method was able to predict the lowest energy metal-centered $d \rightarrow d$ excitations for ferrocene. Surprisingly, the first Rydberg-type $n \rightarrow Ry(3s)$ transition of acetone (**3**) was well reproduced by the XsTDA method. Regarding CT states, the XsTDA method robustly reproduces the TDA results, outperforming sTDA, especially for a large amount of Fock exchange.

The XsTD-DFT scheme performs equivalently well for NLO properties. For a set push-pull π-conjugated systems, we showed that the sTD-DFT method systematically redshifts β_{HRS} resonance enhancements in comparison with the full scheme.[15,65] The XsTD-DFT method corrects this behavior thanks to its consistent treatment of CT states with respect to TD-DFT. Both simplified schemes reproduce the TD-DFT 2PA spectra well for a set of FP chromophores. Note that the XsTD-DFT method provided the best comparison with respect to RI-CC2 excitation energies for the first bright 2PA excited states. Finally, the experimental 2PA spectrum of eGFP was well reproduced by both sB3LYP and XsB3LYP methods using a structural model system.

In summary, we can conclude that the XsTD-DFT/XsTDA methods are robust alternatives to TD-DFT/TDA to compute at a fraction of their computational costs excited state and nonlinear optical response properties. With these new methods, all-atom QC calculations of large systems can now be performed with a similar accuracy as the full scheme. Such methods can also be useful for high throughput screening studies considering large ensembles of molecules.

To complement the range of applications of Xs methods, extra implementations are currently ongoing at UCLouvain. The XsTDA/XsTD-DFT excited state gradient is currently being implemented and support for range-separated hybrids will be available soon. The extension of XsTD-DFT/XsTDA schemes to compute core to valence excitations is an exciting prospect for which we have already gathered interesting results. An extension of XsTD-DFT/XsTDA schemes to use tight-binding ground states for very large systems will be investigated in a near future. A TD-DFT-ris version of XsTD-DFT may be investigated to further reduce the computational cost.

SUPPLEMENTARY MATERIAL

The supplementary material provides basis set effects on the HBI 2PA spectrum, NTOs for the first one photon active electronic transition of acetone, and for B3LYP, PBE0, BHandHLYP, and M06-2X exchange–correlation functionals, excitation energies for the DYE12 benchmark set and absolute deviations at both sTDA and XsTDA levels from TDA.

29 May 2024 06:59:37

Published under an exclusive license by AIP Publishing

ACKNOWLEDGMENTS

M. de W. dedicates this work to his late, beloved partner Coralie Leroy. The authors thank Marilù G. Maraldi for performing the RI-CC2 calculations. This work was supported by the DFG in the framework of the project "Theoretical studies of nonlinear optical properties of fluorescent proteins by novel low-cost quantum chemistry methods" (Grant No. 450959503).

AUTHOR DECLARATIONS

Conflict of Interest

The authors have no conflicts to disclose.

Author Contributions

Marc de Wergifosse: Conceptualization (lead); Funding acquisition (equal); Investigation (lead); Methodology (lead); Software (lead); Writing – original draft (lead); Writing – review & editing (equal). **Stefan Grimme**: Funding acquisition (equal); Methodology (supporting); Software (supporting); Writing – original draft (supporting); Writing – review & editing (equal).

DATA AVAILABILITY

The data that support the findings of this study are available from the corresponding author upon reasonable request.

REFERENCES

[1]S. Grimme, "Calculation of the electronic spectra of large molecules," in *Reviews in Computational Chemistry* (John Wiley & Sons, Ltd, 2004), Chap. III, pp. 153–218.
[2]S. Ghosh, P. Verma, C. J. Cramer, L. Gagliardi, and D. G. Truhlar, Chem. Rev. **118**, 7249 (2018).
[3]D. M. Bishop and P. Norman, "Nonlinear optical materials," in *Handbook of Advanced Electronic and Photonic Materials and Devices*, edited by H. S. Nalwa (Academic Press, Burlington, 2001).
[4]M. G. Papadopoulos, A. J. Sadlej, and J. Leszczynski, *Non-linear Optical Properties of Matter* (Springer, 2006).
[5]M. E. Casida, *Time-Dependent Density Functional Response Theory for Molecules* (World Scientific, 1995), pp. 155–192.
[6]E. K. U. Gross, J. F. Dobson, and M. Petersilka, "Density functional theory of time-dependent phenomena," in *Density Functional Theory II: Relativistic and Time Dependent Extensions*, edited by R. F. Nalewajski (Springer Berlin Heidelberg, Berlin, Heidelberg, 1996), pp. 81–172.
[7]R. Bauernschmitt and R. Ahlrichs, Chem. Phys. Lett. **256**, 454 (1996).
[8]F. Furche, J. Chem. Phys. **114**, 5982 (2001).
[9]C. Adamo and D. Jacquemin, Chem. Soc. Rev. **42**, 845 (2013).
[10]S. Grimme, J. Chem. Phys. **138**, 244104 (2013).
[11]C. Bannwarth and S. Grimme, Comput. Theor. Chem. **1040–1041**, 45 (2014).
[12]T. Risthaus, A. Hansen, and S. Grimme, Phys. Chem. Chem. Phys. **16**, 14408 (2014).
[13]S. Grimme and C. Bannwarth, J. Chem. Phys. **145**, 054103 (2016).
[14]J. Seibert, J. Pisarek, S. Schmitz, C. Bannwarth, and S. Grimme, Mol. Phys. **117**, 1104 (2019).
[15]M. de Wergifosse and S. Grimme, J. Chem. Phys. **149**, 024108 (2018).
[16]M. de Wergifosse, J. Seibert, and S. Grimme, J. Chem. Phys. **153**, 084116 (2020).
[17]M. de Wergifosse and S. Grimme, J. Chem. Phys. **150**, 094112 (2019).
[18]M. de Wergifosse, P. Beaujean, and S. Grimme, J. Phys. Chem. A **126**, 7534 (2022).
[19]M. de Wergifosse, C. Bannwarth, and S. Grimme, J. Phys. Chem. A **123**, 5815 (2019).
[20]M. de Wergifosse, J. Seibert, B. Champagne, and S. Grimme, J. Phys. Chem. A **123**, 9828 (2019).
[21]M. de Wergifosse and S. Grimme, J. Chem. Theory Comput. **16**, 7709 (2020).
[22]R. Rüger, E. van Lenthe, T. Heine, and L. Visscher, J. Chem. Phys. **144**, 184103 (2016).
[23]N. Asadi-Aghbolaghi, R. Rüger, Z. Jamshidi, and L. Visscher, J. Phys. Chem. C **124**, 7946 (2020).
[24]S. Havenridge, R. Rüger, and C. M. Aikens, J. Chem. Phys. **158**, 224103 (2023).
[25]G. Giannone and F. Della Sala, J. Chem. Phys. **153**, 084110 (2020).
[26]Z. Zhou, F. Della Sala, and S. M. Parker, J. Phys. Chem. Lett. **14**, 1968 (2023).
[27]A.-S. Hehn, B. Sertcan, F. Belleflamme, S. K. Chulkov, M. B. Watkins, and J. Hutter, J. Chem. Theory Comput. **18**, 4186 (2022).
[28]Y. Cho, S. J. Bintrim, and T. C. Berkelbach, J. Chem. Theory Comput. **18**, 3438 (2022).
[29]M. de Wergifosse and S. Grimme, J. Phys. Chem. A **125**, 3841 (2021).
[30]K. Nishimoto and N. Mataga, Z. Phys. Chem. **12**, 335 (1957).
[31]K. Ohno, Theor. Chim. Acta **2**, 219 (1964).
[32]G. Klopman, J. Am. Chem. Soc. **86**, 4550 (1964).
[33]R. Pariser and R. G. Parr, J. Chem. Phys. **21**, 466 (1953).
[34]L. Goerigk and S. Grimme, J. Chem. Phys. **132**, 184103 (2010).
[35]N. Zadbuke, S. Shahi, A. Jadhav, and S. Borde, Int. J. Pharm. Pharm. Sci. **8**, 234 (2016).
[36]O. S. Keen, I. Ferrer, E. Michael Thurman, and K. G. Linden, Chemosphere **117**, 316 (2014).
[37]S. K. Fadjimata, A. Rabani, and J. IOSR, Appl. Chem **12**, 51 (2019).
[38]O. Haggag, R. Baer, S. Ruhman, and A. I. Krylov, J. Chem. Phys. **160**, 124111 (2024).
[39]The STDA code can be obtained from: https://github.com/grimme-lab/stda/.
[40]M. Beerepoot, D. Friese, N. List, J. Kongsted, and K. Ruud, Phys. Chem. Chem. Phys. **17**, 19306 (2015).
[41]M. de Wergifosse and B. Champagne, J. Chem. Phys. **134**, 074113 (2011).
[42]A. Zangwill and P. Soven, Phys. Rev. A **21**, 1561 (1980).
[43]S. Hirata and M. Head-Gordon, Chem. Phys. Lett. **314**, 291 (1999).
[44]F. Wang, C. Y. Yam, and G. Chen, J. Chem. Phys. **126**, 244102 (2007).
[45]A. J. Thorvaldsen, K. Ruud, K. Kristensen, P. Jørgensen, and S. Coriani, J. Chem. Phys. **129**, 214108 (2008).
[46]F. Zahariev and M. S. Gordon, J. Chem. Phys. **140**, 18A523 (2014).
[47]S. M. Parker, D. Rappoport, and F. Furche, J. Chem. Theory Comput. **14**, 807 (2018).
[48]T. Husch, A. C. Vaucher, and M. Reiher, Int. J. Quantum Chem. **118**, e25799 (2018).
[49]E. Epifanovsky, A. T. B. Gilbert, X. Feng, J. Lee, Y. Mao, N. Mardirossian, P. Pokhilko, A. F. White, M. P. Coons, A. L. Dempwolff, Z. Gan, D. Hait, P. R. Horn, L. D. Jacobson, I. Kaliman, J. Kussmann, A. W. Lange, K. U. Lao, D. S. Levine, J. Liu, S. C. McKenzie, A. F. Morrison, K. D. Nanda, F. Plasser, D. R. Rehn, M. L. Vidal, Z.-Q. You, Y. Zhu, B. Alam, B. J. Albrecht, A. Aldossary, E. Alguire, J. H. Andersen, V. Athavale, D. Barton, K. Begam, A. Behn, N. Bellonzi, Y. A. Bernard, E. J. Berquist, H. G. A. Burton, A. Carreras, K. Carter-Fenk, R. Chakraborty, A. D. Chien, K. D. Closser, V. Cofer-Shabica, S. Dasgupta, M. de Wergifosse, J. Deng, M. Diedenhofen, H. Do, S. Ehlert, P.-T. Fang, S. Fatehi, Q. Feng, T. Friedhoff, J. Gayvert, Q. Ge, G. Gidofalvi, M. Goldey, J. Gomes, C. E. Gonzalez-Espinoza, S. Gulania, A. O. Gunina, M. W. D. Hanson-Heine, P. H. P. Harbach, A. Hauser, M. F. Herbst, M. Hernandez Vera, M. Hodecker, Z. C. Holden, S. Houck, X. Huang, K. Hui, B. C. Huynh, M. Ivanov, A. Jasz, H. Ji, H. Jiang, B. Kaduk, S. Kahler, K. Khistyaev, J. Kim, G. Kis, P. Klunzinger, Z. Koczor-Benda, J. H. Koh, D. Kosenkov, L. Koulias, T. Kowalczyk, C. M. Krauter, K. Kue, A. Kunitsa, T. Kus, I. Ladjanszki, A. Landau, K. V. Lawler, D. Lefrancois, S. Lehtola, R. R. Li, Y.-P. Li, J. Liang, M. Liebenthal, H.-H. Lin, Y.-S. Lin, F. Liu, K.-Y. Liu, M. Loipersberger, A. Luenser, A. Manjanath, P. Manohar, E. Mansoor, S. F. Manzer, S.-P. Mao, A. V. Marenich, T. Markovich, S. Mason, S. A. Maurer, P. F. McLaughlin, M. F. S. J.

29 May 2024 06:59:37

Published under an exclusive license by AIP Publishing

Menger, J.-M. Mewes, S. A. Mewes, P. Morgante, J. W. Mullinax, K. J. Oosterbaan, G. Paran, A. C. Paul, S. K. Paul, F. Pavosevic, Z. Pei, S. Prager, E. I. Proynov, A. Rak, E. Ramos-Cordoba, B. Rana, A. E. Rask, A. Rettig, R. M. Richard, F. Rob, E. Rossomme, T. Scheele, M. Scheurer, M. Schneider, N. Sergueev, S. M. Sharada, W. Skomorowski, D. W. Small, C. J. Stein, Y.-C. Su, E. J. Sundstrom, Z. Tao, J. Thirman, G. J. Tornai, T. Tsuchimochi, N. M. Tubman, S. P. Veccham, O. Vydrov, J. Wenzel, J. Witte, A. Yamada, K. Yao, S. Yeganeh, S. R. Yost, A. Zech, I. Y. Zhang, X. Zhang, Y. Zhang, D. Zuev, A. Aspuru-Guzik, A. T. Bell, N. A. Besley, K. B. Bravaya, B. R. Brooks, D. Casanova, J.-D. Chai, S. Coriani, C. J. Cramer, G. Cserey, A. E. DePrince, R. A. DiStasio, A. Dreuw, B. D. Dunietz, T. R. Furlani, W. A. Goddard, S. Hammes-Schiffer, T. Head-Gordon, W. J. Hehre, C.-P. Hsu, T.-C. Jagau, Y. Jung, A. Klamt, J. Kong, D. S. Lambrecht, W. Liang, N. J. Mayhall, C. W. McCurdy, J. B. Neaton, C. Ochsenfeld, J. A. Parkhill, R. Peverati, V. A. Rassolov, Y. Shao, L. V. Slipchenko, T. Stauch, R. P. Steele, J. E. Subotnik, A. J. W. Thom, A. Tkatchenko, D. G. Truhlar, T. Van Voorhis, T. A. Wesolowski, K. B. Whaley, H. L. Woodcock, P. M. Zimmerman, S. Faraji, P. M. W. Gill, M. Head-Gordon, J. M. Herbert, and A. I. Krylov, J. Chem. Phys. **155**, 084801 (2021).

[50] Q. Sun, J. Comput. Chem. **36**, 1664 (2015).

[51] T. Kosaka and T. Wakabayashi, Heterocycles **41**, 477 (1995).

[52] K. D. Nanda and A. I. Krylov, J. Chem. Phys. **142**, 064118 (2015).

[53] M. de Wergifosse, E. Botek, E. De Meulenaere, K. Clays, and B. Champagne, J. Phys. Chem. B **122**, 4993 (2018).

[54] M. Drobizhev, N. S. Makarov, S. E. Tillo, T. E. Hughes, and A. Rebane, Nat. Methods **8**, 393 (2011).

[55] K. Aidas, C. Angeli, K. L. Bak, V. Bakken, R. Bast, L. Boman, O. Christiansen, R. Cimiraglia, S. Coriani, P. Dahle, E. K. Dalskov, U. Ekström, T. Enevoldsen, J. J. Eriksen, P. Ettenhuber, B. Fernández, L. Ferrighi, H. Fliegl, L. Frediani, K. Hald, A. Halkier, C. Hättig, H. Heiberg, T. Helgaker, A. C. Hennum, H. Hettema, E. Hjertenæs, S. Høst, I. Høyvik, M. F. Iozzi, B. Jansík, H. J. A. Jensen, D. Jonsson, P. Jørgensen, J. Kauczor, S. Kirpekar, T. Kjærgaard, W. Klopper, S. Knecht, R. Kobayashi, H. Koch, J. Kongsted, A. Krapp, K. Kristensen, A. Ligabue, O. B. Lutnæs, J. I. Melo, K. V. Mikkelsen, R. H. Myhre, C. Neiss, C. B. Nielsen, P. Norman, J. Olsen, J. M. H. Olsen, A. Osted, M. J. Packer, F. Pawlowski, T. B. Pedersen, P. F. Provasi, S. Reine, Z. Rinkevicius, T. A. Ruden, K. Ruud, V. V. Rybkin, P. Sałek, C. C. M. Samson, A. S. de Merás, T. Saue, S. P. A. Sauer, B. Schimmelpfennig, K. Sneskov, A. H. Steindal, K. O. Sylvester-Hvid, P. R. Taylor, A. M. Teale, E. I. Tellgren, D. P. Tew, A. J. Thorvaldsen, L. Thøgersen, O. Vahtras, M. A. Watson, D. J. D. Wilson, M. Ziolkowski, and H. Ågren, Wiley Interdiscip. Rev.: Comput. Mol. Sci. **4**, 269 (2014).

[56] Dalton, a molecular electronic structure program, release dalton2018.0 (2018), see http://daltonprogram.org.

[57] TURBOMOLE V7.6 2021, a development of university of karlsruhe and forschungszentrum karlsruhe GmbH, 1989-2007, TURBOMOLE GmbH, since 2007, available from https://www.turbomole.org.

[58] A. Willetts, J. E. Rice, D. M. Burland, and D. P. Shelton, J. Chem. Phys. **97**, 7590 (1992).

[59] J. A. Pople, D. L. Beveridge, and P. A. Dobosh, J. Chem. Phys. **47**, 2026 (1967).

[60] J. A. Pople, Trans. Faraday Soc. **49**, 1375 (1953).

[61] D. Jacquemin, V. Wathelet, E. A. Perpète, and C. Adamo, J. Chem. Theory Comput. **5**, 2420 (2009).

[62] D. J. Tozer, J. Chem. Phys. **119**, 12697 (2003).

[63] A. J. Cohen, P. Mori-Sánchez, and W. Yang, Chem. Rev. **112**, 289 (2012).

[64] L. Kronik, T. Stein, S. Refaely-Abramson, and R. Baer, J. Chem. Theory Comput. **8**, 1515 (2012).

[65] S. Löffelsender, P. Beaujean, and M. de Wergifosse, "Simplified quantum chemistry methods to evaluate non-linear optical properties of large systems," WIREs Comput. Mol. Sci. **14**, e1695 (2023).

[66] M. W. Schmidt, K. K. Baldridge, J. A. Boatz, S. T. Elbert, M. S. Gordon, J. H. Jensen, S. Koseki, N. Matsunaga, K. A. Nguyen, S. Su, T. L. Windus, M. Dupuis, and J. A. Montgomery, J. Comput. Chem. **14**, 1347 (1993).

[67] M. S. Gordon and M. W. Schmidt, in *Theory and Applications of Computational Chemistry*, edited by C. E. Dykstra, G. Frenking, K. S. Kim, and G. E. Scuseria (Elsevier, Amsterdam, 2005), pp. 1167–1189.

[68] M. Chołuj, M. M. Alam, M. T. P. Beerepoot, S. P. Sitkiewicz, E. Matito, K. Ruud, and R. Zaleśny, J. Chem. Theory Comput. **18**, 1046 (2022).

[69] M. Véril, A. Scemama, M. Caffarel, F. Lipparini, M. Boggio-Pasqua, D. Jacquemin, and P.-F. Loos, WIREs Comput. Mol. Sci. **11**, e1517 (2021).

[70] P.-F. Loos, M. Comin, X. Blase, and D. Jacquemin, J. Chem. Theory Comput. **17**, 3666 (2021).

[71] P.-F. Loos and D. Jacquemin, J. Phys. Chem. A **125**, 10174 (2021).

29 May 2024 06:59:37

Published under an exclusive license by AIP Publishing